

Joint Unsupervised Learning of Optical Flow and Depth by Watching Stereo Videos

Yang Wang¹ Zhenheng Yang² Peng Wang¹ Yi Yang¹ Chenxu Luo³ Wei Xu¹

¹Baidu Research ² University of Southern California ³Johns Hopkins University

{wangyang59, wangpeng54, yangyi05, wei.xu}@baidu.com zhenheny@usc.edu chenxuluo@jhu.edu

Abstract

Learning depth and optical flow via deep neural networks by watching videos has made significant progress recently. In this paper, we jointly solve the two tasks by exploiting the underlying geometric rules within stereo videos. Specifically, given two consecutive stereo image pairs from a video, we first estimate depth, camera ego-motion and optical flow from three neural networks. Then the whole scene is decomposed into moving foreground and static background by comparing the estimated optical flow and rigid flow derived from the depth and ego-motion. We propose a novel consistency loss to let the optical flow learn from the more accurate rigid flow in static regions. We also design a rigid alignment module which helps refine ego-motion estimation by using the estimated depth and optical flow. Experiments on the KITTI dataset show that our results significantly outperform other state-of-the-art algorithms. Source codes can be found at <https://github.com/baidu-research/UnDepthflow>

Introduction

Learning 3D scene geometry and scene flow from videos is an important problem in computer vision. It has numerous applications in different areas, including autonomous driving (Menze and Geiger 2015), robot navigation (DeSouza and Kak 2002) and video analysis (Tsai, Yang, and Black 2016). However, collecting ground truths for these tasks could be difficult.

Lots of efforts and progresses have been made recently in unsupervised learning of depth (Zhou et al. 2017b) and optical flow (Ren et al. 2017) using neural network based methods. Both approaches have their own advantages and limitations. The depth approach exploits the geometric structure of the scene and decomposes the problem into two orthogonal ones. It can also leverage more frames in time and/or stereo information to add more constraints into the solution (Li et al. 2017). However, it assumes the entire scene is static and thus has difficulty dealing with moving objects. On the other hand, the optical flow approach can handle moving objects in principle. But it has difficulty in the region of complex structures and occluded areas.

Based on the above observation, we propose a framework to jointly learn depth and optical flow by mutually leveraging the advantages from each other. We first estimate the moving region by comparing the optical flow and the rigid

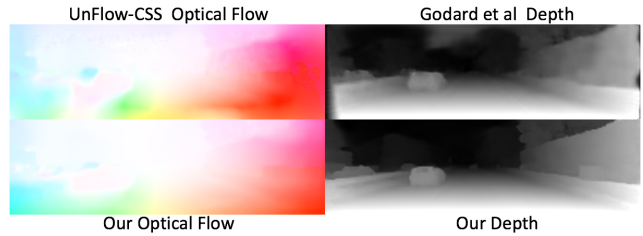


Figure 1: Visualization of the comparison between our method and state-of-the-art unsupervised methods (Meister, Hur, and Roth 2018; Godard, Mac Aodha, and Brostow 2017). It can be seen that our method produces smoother results in planes and sharper boundaries.

flow induced by the camera motion. With the estimated moving region mask, depth and camera motion estimations can be improved by not considering the reconstruction loss in the moving region. On the other hand, the optical flow performance can also be improved by learning from the more accurate rigid flow in the static region (see Fig.1 for an example).

Some works (Ranjan et al. 2018; Yang et al. 2018; Yin and Shi 2018) have tried to learn the two tasks jointly with monocular videos. We however decide to use stereo pairs as input to our framework for the following reasons. On one hand, the performance of the unsupervised depth estimation is much better with stereo input compared to monocular-based methods (Godard, Mac Aodha, and Brostow 2017). Given the fact that stereo cameras have a wide range applications in real world scenarios (e.g. on smart-phones), we feel that unsupervised learning of depth with stereo pairs itself is a topic worth studying. Additionally, with stereo inputs both depth and visual odometry can recover the absolute scale which could be more useful in certain tasks like self-localization.

On the other hand, the higher quality stereo-based depth can be utilized to improve estimations of other quantities with our newly designed modules. It has been noticed that directly estimating camera motion from two images can be difficult, because it would implicitly require the network to also estimate the scene structure (Wang and Buenaposada 2018). Based on the high quality stereo-based depth, we pro-

pose a rigid alignment module to facilitate the camera motion estimation. More concretely, we refine the camera motion by rigidly aligning two consecutive point clouds whose correspondences are established through optical flow. Additionally, with the high quality depth and better ego-motion estimations, the rigid flow derived from ego-motion is much more accurate than monocular-based ones. Therefore we propose a flow consistency module which lets the optical flow learn from the rigid flow in the static regions.

In summary, the key contributions of this work are: 1) a unified framework for unsupervised learning of optical flow, depth, visual odometry and motion segmentation with stereo videos. 2) a rigid alignment module for refining the ego-motion estimation. 3) a flow consistency module for learning optical flow from rigid flow. Our method improves the state-of-the-art performance of unsupervised learning of depth and optical flow by a large margin. On KITTI 2012, for example, our method reduces the optical flow error from previous state-of-the-art unsupervised method (Meister, Hur, and Roth 2018) by 50%, and reaches the performance of the supervised methods.

Related Work

Unsupervised Learning of Depth and Ego-motion

The unsupervised learning of depth and ego-motion through monocular videos using deep learning was first achieved in (Zhou et al. 2017b). Later, different methods were proposed to improve the results. (Yang et al. 2017) added a depth-normal consistency term. To make the visual odometry more accurate, (Wang and Buenaposada 2018) used direct method to refine the pose estimation, and (Mahjourian, Wicke, and Angelova 2018) proposed a 3D ICP loss. Our rigid alignment module tries to tackle the same issue and is similar to (Mahjourian, Wicke, and Angelova 2018). The difference is that we use optical flow to find the point cloud correspondence in a single pass while they used nearest neighbor method to iteratively refine the correspondences which would require longer time.

Another line of work used stereo images to learn the depth where the relative pose of the camera is fixed and known (Garg et al. 2016). (Godard, Mac Aodha, and Brostow 2017) introduced a left-right consistency loss for improvement. (Zhan et al. 2018) and (Li et al. 2017) combined stereo pairs and monocular video matching together. The aforementioned works all use a monocular image as input to estimate the depth although stereo images are needed at the training time. (Zhou et al. 2017a; Godard, Mac Aodha, and Brostow 2017) used stereo pairs as input to estimate the depth which is the same as our approach, and have much better performance compared to monocular input methods.

Unsupervised Learning of Optical Flow

The unsupervised learning of optical flow with a neural network was first introduced in (Ren et al. 2017) and (Jason, Harley, and Derpanis 2016). Later, (Wang et al. 2018) and (Meister, Hur, and Roth 2018) improved the results by explicitly handling the occlusions. However, there is still a gap for the unsupervised learning methods to reach the

performance of the supervised methods (Ilg et al. 2017; Sun et al. 2017).

Joint Learning of Depth and Flow

There are a large body of works on scene flow estimation using traditional variational-based methods (Vedula et al. 1999). Here we only list some of the most recent ones. (Menze and Geiger 2015) modeled the whole scene as a collection of piece-wise planes based on superpixels with rigid motions. (Behl et al. 2017) improved upon it by adding recognition and instance segmentation information. (Wulff, Sevilla-Lara, and Black 2017) segmented the scene into static and moving regions where the optical flow in the static region is refined using the plane+parallax method. The framework in (Taniai, Sinha, and Sato 2017) is similar to ours, in which depth, ego-motion, optical flow and motion segmentation are optimized together. The major limitation of traditional methods is computation time.

There are also works on combining neural network based unsupervised learning of depth and optical flow. (Yin and Shi 2018) used a residual FlowNet to refine the rigid flow from depth and ego-motion to the full optical flow, but it did not account for the moving objects in the rigid flow estimation. (Yang et al. 2018) handled moving objects explicitly with motion segmentation but did not use depth to improve optical flow. (Ranjan et al. 2018) pieced the optical flow and rigid flow together to explain the whole scene in a adversarial collaboration. Their method requires iterative training and forwarding all three networks to obtain the optical flow, while our method can be simply trained together and optical flow estimation only depends on one network.

Method

We will first give an overview of our method and then describe specific components in details.

Overall Structure

The overall schematic structure of our method is shown in Fig.2. During training, the inputs to our system are two consecutive stereo pairs (L_1, R_1, L_2, R_2 where L_1 denotes the left image at time t_1 and so forth). It has three major neural network modules: one for estimating optical flow (F_{12}^{opt}) between two consecutive left images (PWC-Flow), one for estimating relative camera pose (T_{12}) between two consecutive left images (MotionNet), and one for estimating disparity between stereo pair of images (PWC-Disp). With a known stereo baseline B and horizontal focal length f_x , The disparity (d) can be converted into absolute scale depth $D = Bf_x/d$.

By combining D_1 and T_{12} , one can calculate the flow induced by the camera motion. We label this flow as rigid flow (F_{12}^{rig}) since it assumes that the whole scene is static (this part of calculation graph is not depicted in Fig.2 due to the space constraint). Then the rigid alignment module will refine the MotionNet estimated pose T_{12} to be T'_{12} by using the optical flow and depths. Similarly, we can get the refined rigid flow ($F_{12}^{rig'}$) by combining D_1 and T'_{12} . In the next step,

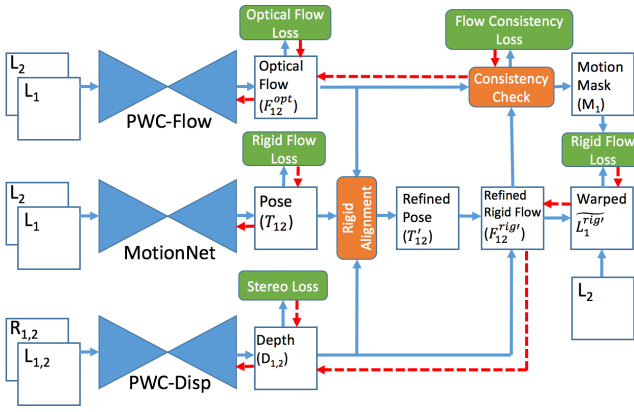


Figure 2: Schematic overview of our method. It learns to estimate depth, optical flow, camera motion, and motion segmentation from two consecutive stereo pairs in an unsupervised manner. The different components of our unsupervised loss are depicted in green boxes. Our proposed rigid alignment module refines the estimated camera pose, and the flow consistency check between optical flow and rigid flow gives the motion segmentation mask. The red arrows indicate the gradient back-propagation directions.

we perform a consistency check between F_{12}^{opt} and $F_{12}^{rig'}$. The region is labeled as moving foreground (M_1) if the difference between the two flows is greater than a threshold, and the rest of image is labeled as static background.

The whole system is trained in an unsupervised manner. The unsupervised loss for flow F_{12}^{opt} follows the method in (Wang et al. 2018) which consists of an occlusion-aware reconstruction loss and a smoothness loss. The unsupervised loss for depth D follows the method in (Godard, Mac Aodha, and Brostow 2017) which consists of a reconstruction loss, a smoothness loss and a left-right consistency loss. We also add a reconstruction loss between L_1 and \tilde{L}_1^{rig} ($\tilde{L}_1^{rig'}$) in the static region, where \tilde{L}_1^{rig} ($\tilde{L}_1^{rig'}$) is obtained by warping L_2 using F_{12}^{rig} ($F_{12}^{rig'}$). In addition, we have a consistency loss between F_{12}^{opt} and $F_{12}^{rig'}$ in the static region ($1 - M_1$). The directions of gradient back-propagations are labeled as red arrows in Fig. 2.

Network Architecture Design

The structure of PWC-Flow follows the design in (Sun et al. 2017) because of its lightweight and excellent supervised optical flow performance.

The structure of MotionNet is similar to the one used in (Zhou et al. 2017b) except that the input to the network has only two consecutive images instead of three or five. We add more convolutional layers into our MotionNet because we find that it gives better pose estimation when using only two consecutive images.

Since optical flow and disparity estimations are both problems of finding correspondence and indeed very similar in nature, we modify PWC-net to exploit the spe-

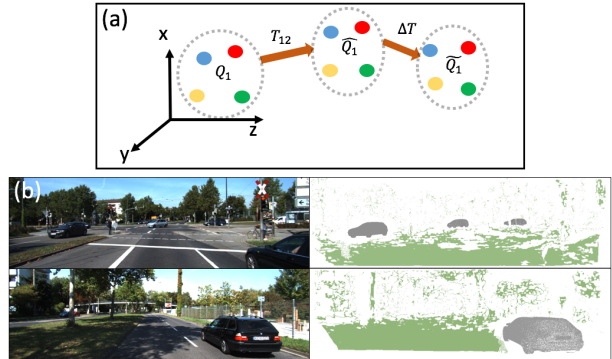


Figure 3: (a) Schematic illustration of the rigid alignment module. Each of the point clouds Q_1 , \widehat{Q}_1 and \widetilde{Q}_1 is depicted by colored balls enclosed in a dashed circle. The color of the balls encodes correspondences between point clouds. (b) Visualization of the region chosen for rigid alignment. Left column plots left images (L_1). Right column plots the region used in the rigid alignment module (i.e., region R described in Eq. 3) in green overlaying on the ground truth moving object mask in black.

cial structure of the disparity estimation and turn it into PWC-Disp. PWC-Disp only searches the horizontal direction when calculating the cost volume, only estimates the horizontal component of the flow (forcing the vertical component to be zero), and forces the flow to be negative (so that $\text{disp} = -\text{flow}_x/\text{image_width}$ is always positive). We choose PWC-Disp as our network to estimate disparity due to its lightweight.

Rigid Alignment Module

During rigid alignment, we first transform the points in 2D image space to 3D point cloud using Eq.1, where $P_t(i, j)$ is the homogenous coordinate of the pixel at the location of (i, j) of image L_t , K is the camera intrinsic matrix, $D_t(i, j)$ is the estimated depth of L_t at location (i, j) and $Q_t(i, j)$ is the corresponding 3D coordinate (i.e., x, y, z) of the pixel.

$$Q_t(i,j) = D_t(i,j)K^{-1}P_t(i,j) \quad (1)$$

We then transform Q_1 into $\widehat{Q}_1 = T_{12}Q_1$, where T_{12} is the initial estimation of the pose from MotionNet, and \widehat{Q}_1 is the 3D coordinate of the point in L_1 at the time of t_2 . We can also obtain a similar quantity \widetilde{Q}_1 by warping Q_2 back to the frame of t_1 using optical flow F_{12}^{opt} . This is the same bilinear sampling method used to warp the image L_2 back to \widetilde{L}_1 (see Eq.2). This warping step is to establish correspondence so that $\widehat{Q}_1(i, j)$ corresponds to $\widetilde{Q}_1(i, j)$.

$$\begin{aligned} \widetilde{Q}_1(i, j) = & \sum_{m=1}^W \sum_{n=1}^H Q_2(m, n) \max(0, 1 - |m - (i + F_{12}^x(i, j))|) \\ & \cdot \max(0, 1 - |n - (j + F_{12}^y(i, j))|) \end{aligned} \quad (2)$$

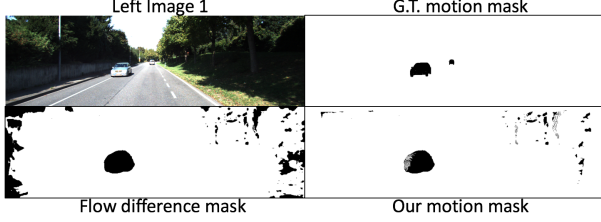


Figure 4: An example of motion mask estimation. After taking away the occluded area, the estimated motion mask (bottom right) improved compared to the mask obtained solely by thresholding the flow difference (bottom left).

If everything is perfectly accurate, \hat{Q}_1 should be equal to \tilde{Q}_1 in the static and non-occluded region of the scene. Therefore we can refine our pose estimation by rigidly aligning these two point clouds (a schematic illustration of the rigid alignment module can be seen in Fig. 3a). Concretely, we estimate the refinement pose ΔT by minimizing the distance between $\Delta T \hat{Q}_1$ and \tilde{Q}_1 in selected region R :

$$\Delta T = \underset{\Delta T}{\operatorname{argmin}} \sum_R \|\Delta T \hat{Q}_1 - \tilde{Q}_1\|^2 \quad (3)$$

This minimization is performed exactly using the method described in (Besl and McKay 1992) which involves solving an SVD problem. We choose region R to be 25% of the points in the non-occluded area that have the smallest distance between \hat{Q}_1 and \tilde{Q}_1 . By doing this, we try to exclude points in the moving region since they tend to have larger distances between \hat{Q}_1 and \tilde{Q}_1 . Examples of the region R can be seen in Fig. 3b which shows clear separation between region R (green) and moving objects (black). On the 200 KITTI 2015 training images, only 1.4% of the moving object pixels fall into the region R . The non-occluded area (O_1) is estimated using reverse optical flow (F_{21}^{opt}) as described in (Wang et al. 2018). The refined pose can be obtained by combining T_{12} and ΔT :

$$T'_{12} = \Delta T \times T_{12} \quad (4)$$

Flow Consistency and Motion Segmentation

With the refined pose T'_{12} in hand, we can calculate the rigid flow induced by camera motion to be:

$$F_{12}^{\text{rig}'} = K T'_{12} D_1 K^{-1} P_1 - P_1 \quad (5)$$

If F_{12}^{opt} and $F_{12}^{\text{rig}'}$ were both accurate, their values should match in the static region and differ in the moving region. Based on this observation, we estimate the moving region to be:

$$M_1 = \mathbb{1}(\|F_{12}^{\text{opt}} - F_{12}^{\text{rig}'}\| > \delta \cap O_1) \quad (6)$$

We also force the estimated moving region to be in the non-occluded area (O_1) because F_{12}^{opt} is less accurate in the occluded area which could lead to false positives (see Fig.4 for an example).

Unsupervised Losses

The unsupervised loss of our method is composed of four components: optical flow loss (l_{opt}), stereo loss (l_{st}), rigid flow loss (l_{rig}), and flow consistency loss (l_{con}). We will describe each loss in details below.

Optical Flow Loss The optical flow loss is similar to the one described in (Wang et al. 2018) which has an occlusion-aware reconstruction loss term ($l_{\text{opt-ph}}$) and a smoothness loss term ($l_{\text{opt-sm}}$). $l_{\text{opt-ph}}$ is a weighted average between the SSIM-based loss and the absolute photometric difference loss on the non-occluded area, where \tilde{L}_1^{opt} is the reconstruction of L_1 by warping L_2 using F_{12}^{opt} . $l_{\text{opt-sm}}$ is the average absolute value of the edge-weighted second-order derivative of the optical flow on the moving foreground region. The constraint for the optical flow on the static region will be provided in the consistency loss part.

$$\begin{aligned} l_{\text{opt-ph}} &= \Psi(L_1, \tilde{L}_1^{\text{opt}}, O_1) \\ &= \frac{1}{\sum_{i,j} O_1} [\sum_{i,j} (\alpha \frac{1 - \text{SSIM}(L_1, \tilde{L}_1^{\text{opt}})}{2} + (1 - \alpha)|L_1 - \tilde{L}_1^{\text{opt}}|) \cdot O_1] \\ l_{\text{opt-sm}} &= \frac{1}{N} \sum_{i,j} \sum_{d \in x,y} |\partial_d^2 F_{12}^{\text{opt}}(i,j)| e^{-\beta |\partial_d L_1(i,j)|} \cdot M_1 \end{aligned}$$

Stereo Loss The stereo loss is the same as in (Godard, Mac Aodha, and Brostow 2017).

Rigid Flow Loss The rigid flow loss is a reconstruction loss term applied on \tilde{L}_1^{rig} and $\tilde{L}_1^{\text{rig}'}$ in the static region. \tilde{L}_1^{rig} ($\tilde{L}_1^{\text{rig}'}$) is the reconstruction of L_1 by warping L_2 using F_{12}^{rig} ($F_{12}^{\text{rig}'}$).

$$\begin{aligned} l_{\text{rig}} &= l_{\text{rig}}^1 + l_{\text{rig}}^2 \\ &= \Psi(L_1, \tilde{L}_1^{\text{rig}}, O_1 \cdot (1 - M_1)) + \Psi(L_1, \tilde{L}_1^{\text{rig}'}, O_1 \cdot (1 - M_1)) \end{aligned}$$

Here we also include l_{rig}^1 into the loss because the rigid alignment module is non-differentiable and we need l_{rig}^1 to supervise the MotionNet.

Flow Consistency Loss From the experimental result below, we find that $F_{12}^{\text{rig}'}$ is more accurate than F_{12}^{opt} in the static region. Therefore we decide to use $F_{12}^{\text{rig}'}$ to guide the learning of F_{12}^{opt} using the following one-sided consistency loss term, where SG stands for stop-gradient.

$$l_{\text{con}} = \frac{1}{N} \sum_{i,j} |F_{12}^{\text{opt}}(i,j) - SG(F_{12}^{\text{rig}'}(i,j))| \cdot (1 - M_1(i,j))$$

Total Loss The total loss is a weighted sum of the aforementioned losses:

$$\begin{aligned} l_{\text{total}} &= l_{\text{opt-ph}} + \lambda_{\text{sm}} l_{\text{opt-sm}} + \lambda_{\text{st}} l_{\text{st}} \\ &\quad + \lambda_{\text{rig}} l_{\text{rig}} + \lambda_{\text{con}} l_{\text{con}} \end{aligned}$$

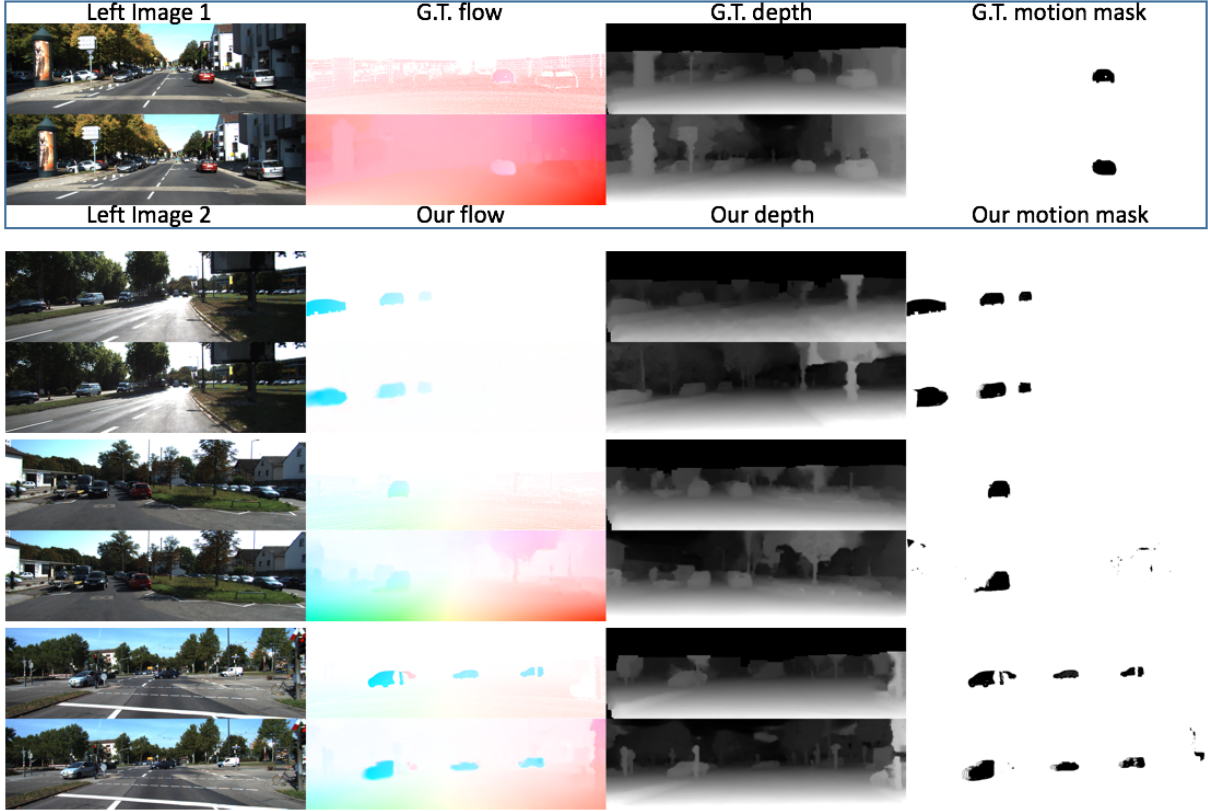


Figure 5: Qualitative results of our method. Each instance of examples is plotted in two rows, including left image 1 (L_1), left image 2 (L_2), ground truth optical flow, our estimated optical flow (F_{12}^{opt}), ground truth depth, our estimated depth (D_1), ground truth motion mask, and our estimated motion mask (M_1).

Experiments

We evaluate our methods on the KITTI dataset, and compare our results to existing supervised and unsupervised methods on the tasks of depth, optical flow, camera motion, scene flow and motion segmentation.

Training Details The whole training process contains three stages. In the first stage, we train the PWC-Flow network using $l_{opt-ph} + \lambda_{sm} l_{opt-sm}$. In the second stage, we then train the PWC-Disp and MotionNet networks using $\lambda_{st} l_{st} + \lambda_{rig} l_{rig}^1$ without the rigid alignment and flow consistency check modules (i.e., M_1 is set to zero everywhere). This is because the rigid alignment and flow consistency check only work when both depths and optical flows are estimated reasonably accurate. In the third stage, everything is trained together using the total loss l_{total} .

In all of three stages, we used Adam optimizer (Kingma and Ba 2014) with $\beta_1 = 0.9$ and $\beta_2 = 0.999$. The learning rate is set to be 10^{-4} . The hyperparameters $[\lambda_{sm}, \lambda_{st}, \lambda_{rig}, \lambda_{con}, \alpha, \beta, \delta]$ are set to be $[10.0, 1.0, 10.0, 0.01, 0.85, 10.0, 3.0]$.

During training, we use batch size of 4. In each stage, we train for around 15 epochs and choose the model with best validation accuracy for the start of training next stage. Images are scaled to have values between 0 and 1, and size

of 832×256 . The only data augmentation we perform is random left-right flipping and random time order switching (swapping t_1 and t_2).

Dataset For the depth, optical flow, scene flow and motion segmentation tasks, we train our network using all of the raw data in KITTI excluding the scenes appeared in KITTI 2015 (Menze and Geiger 2015) so that we could use the training set of KITTI 2015 as our validation set, and compare with existing methods. None of KITTI 2012 (Geiger, Lenz, and Urtasun 2012) data exists in the KITTI raw data so we could also evaluate our model on it. Notice that KITTI 2012 dataset only contains static scenes. For the odometry task, we use sequences 00-08 as training data and sequences 09, 10 as validation data. All of our models are trained in a pure unsupervised manner.

Optical Flow Evaluation We evaluate our method on the optical flow estimation task using both KITTI 2012 and KITTI 2015, and the quantitative results are shown in Table 1. Ours (PWC-only) is our baseline model after training PWC-Flow using only the loss l_{opt} in the first stage. We could see that it is already better than state-of-the-art unsupervised optical flow method UnFlow-CSS (Meister, Hur, and Roth 2018) demonstrating the effectiveness of our occlusion-aware loss and PWC network structure.

Method	Train Stereo	Test Stereo	Supervised	KITTI 2012				KITTI 2015			
				train Noc	train Occ	train All	test All	train move	train static	train all	test all
Flownet2			✓	—	—	4.09	—	—	—	10.06	—
Flownet2+ft			✓	—	—	(1.28)	1.8	—	—	(2.3)	11.48%
PWC-Net			✓	—	—	4.14	—	—	—	10.35	—
PWC-Net+ft			✓	—	—	(1.45)	1.7	—	—	(2.16)	9.60%
UnFlow-CSS				1.26	—	3.29	—	—	—	8.10	—
Geonet				—	—	—	—	—	—	10.81	—
(Ranjan et al. 2018)				—	—	—	—	6.35	6.16	7.76	—
(Wang et al. 2018)				—	—	3.55	4.2	—	—	8.88	31.2%
Ours (PWC-only)				1.15	11.2	2.68	—	5.92	7.68	7.88	—
Ours (Ego-motion)	✓	✓		2.27	6.67	2.86	—	35.9	4.53	11.9	—
Ours (Ego+align)	✓	✓		1.46	4.88	1.93	—	36.5	2.99	10.69	—
Ours (Full)	✓			1.04	5.18	1.64	1.8	5.30	5.39	5.58	18.00 %
Ours (mono-Ego-motion)	✓			2.78	8.47	3.58	—	34.8	6.56	13.5	—

Table 1: Quantitative evaluation on the optical flow task. The numbers reported here are all average end-point-error (EPE) except for the last column (KITTI2015 test) which is the percentage of erroneous pixels (Fl-all). A pixel is considered to be correctly estimated if the flow end-point error is $<3\text{px}$ or $<5\%$. The upper part of the table contains supervised methods and lower part of the table contains unsupervised methods. For all metrics, smaller is better. The best results from each category are boldfaced.

Method	Train Stereo	Test Stereo	Supervised	Lower the better					Higher the better		
				Abs Rel	Sq Rel	RMSE	RMSE log	D1-all	$\delta < 1.25$	$\delta < 1.25^2$	$\delta < 1.25^3$
(Zhou et al. 2017b)				0.216	2.255	7.422	0.299	—	0.686	0.873	0.951
DDVO				0.151	1.257	5.583	0.228	—	0.810	0.936	0.974
(Godard et al. 2017)	✓			0.124	1.388	6.125	0.217	30.27%	0.841	0.936	0.975
(Yang et al. 2018)	✓			0.109	1.004	6.232	0.203	—	0.853	0.937	0.975
(Godard et al. 2017)	✓	✓		0.068	0.835	4.392	0.146	9.194%	0.942	0.978	0.989
Ours (Stereo-only)	✓	✓		0.060	0.833	4.187	0.135	7.073%	0.955	0.981	0.990
Ours (Ego-motion)	✓	✓		0.052	0.593	3.488	0.121	6.431%	0.964	0.985	0.992
Ours (Full)	✓	✓		0.049	0.515	3.404	0.121	5.943%	0.965	0.984	0.992
PSMNet	✓	✓	✓	—	—	—	—	1.83%	—	—	—

Table 2: Quantitative evaluation of the depth task on the KITTI2015 training set. Since depths and disparities are directly related to each other, we put them into the same table. Abs Rel, Sq Rel, RMSE, RMSE log, $\delta < 1.25$, 1.25^2 , 1.25^3 are standard metrics for depth evaluation. We capped the depth to be between 0-80 meters to compare with existing literatures. D1-all is the error rate of the disparity.

Ours (Ego-motion) is the result of rigid flow F_{12}^{rig} at the end of the second stage training. The rigid flow is shown to be better than the previous general optical flow in occluded (6.67 vs. 11.2) and static (4.53 vs. 7.68) regions. This observation is consistent with our assumption about the advantage of the rigid flow in those areas, and provides motivation for our proposed flow consistency loss (l_{con}). The rigid flow is much worse in moving regions which is expected since it is only supposed to be accurate in static regions.

Ours (Ego+align) is the result of refined rigid flow $F_{12}^{rig'}$ at the beginning of the third stage training (i.e., its only difference from Ours (Ego-motion) is applying the rigid alignment module without any changes to the network parameters). The result shows that the rigid alignment module significantly improves the rigid flow in static regions (1.93 vs. 2.86 and 2.99 vs. 4.53).

By guiding the optical flow F_{12}^{opt} using $F_{12}^{rig'}$ in static regions, we reach our final model Ours (Full) for optical flow estimation at the end of the third training stage. It is still

worse than $F_{12}^{rig'}$ in static regions but has the best overall performance. For KITTI 2012, our method reduces the error from previous state-of-the-art unsupervised method (Meister, Hur, and Roth 2018) by 50%, and reaches the performance of the supervised methods, which demonstrates the benefits of our proposed method and the utilization of stereo data. For KITTI 2015, our method also outperforms previous unsupervised methods by a large margin, but still falls behind supervised methods. Although our method needs extra stereo data during training compared to previous methods, it only requires two consecutive monocular images during the test time. Qualitative examples of our estimated optical flow can be seen in Fig. 5.

We also conduct an ablation study using only monocular image as input to the depth network and follow the same training process as Ours (Ego-motion). The evaluation result is shown as Ours (mono-Ego-motion). We can see that the monocular model produce much worse rigid flow compared to the stereo model, and thus would not provide as much benefits for guiding the optical flow learning.

Method	frames	Stereo	Sequence 09	Sequence 10
ORB-SLAM(Full)	All		0.014 \pm 0.008	0.012 \pm 0.011
(Zhou et al. 2017b)	5		0.016 \pm 0.009	0.013 \pm 0.009
Geonet	5		0.012 \pm 0.007	0.012 \pm 0.009
Mahjourian <i>et al.</i>	3		0.013 \pm 0.010	0.012 \pm 0.011
(Ranjan et al. 2018)	5		0.012 \pm 0.007	0.012 \pm 0.008
Ours (Ego-motion)	2	✓	0.023 \pm 0.010	0.022 \pm 0.016
Ours (Ego+align)	2	✓	0.013 \pm 0.006	0.015 \pm 0.010
Ours (Full)	2	✓	0.012 \pm 0.006	0.013 \pm 0.008

Table 3: Quantitative evaluation of the odometry task using the metric of the absolute trajectory error.

Method	Sequence 09		Sequence 10	
	$t_{err}\%$	$r_{err}(\text{°}/100)$	$t_{err}\%$	$r_{err}(\text{°}/100)$
ORB-SLAM(Full)	15.30	0.26	3.68	0.48
(Zhan et al. 2018)	11.92	3.60	12.62	3.43
Ours (Ego-motion)	13.98	5.36	19.67	9.13
Ours (Ego+align)	8.15	3.02	9.54	4.80
Ours (Full)	5.21	1.80	5.20	2.18

Table 4: Quantitative evaluation of the odometry task using the metric of average translational and rotational errors. Numbers of ORB-SLAM (Full) are adopted from (Zhan et al. 2018).

Depth Evaluation We evaluate our depth estimation on the KITTI 2015 training set and the results are shown in Table 2. Ours (Stereo-only) is the PWC-Disp network trained using only stereo images and the loss l_{st} . This is not part of our three training stages but only serves as an ablation study. Ours (Stereo-only) is already better than the best stereo-based unsupervised learning method (Godard, Mac Aodha, and Brostow 2017) demonstrating the effectiveness of our PWC-Disp network. We can observe that stereo-based methods still have much better performance than monocular methods.

Ours (Ego-motion) is the model at the end of our second training stage. After adding the data of time consecutive images into the training, the depth accuracy improves, especially in the large distance regions (0.593 vs. 0.833).

Ours (Full) model improves further after adding the rigid alignment module and explicitly handling the moving regions. However, its performance is still relatively far away from the supervised method like PSMNet (Chang and Chen 2018). The depth and scene flow evaluation on KITTI 2015 test set can be found in the supplementary materials. The qualitative results of our estimated depth can be seen in Fig. 5.

Odometry Evaluation We evaluate our odometry performance using two existing metrics. One metric is proposed in (Zhou et al. 2017b) which measures the absolute trajectory error averaged over all overlapping 5-frame snippets after a single factor rescaling with the ground truth. The results for this metric are shown in Table. 3. Our method uses only two frames as input to the MotionNet to predict the motion between two frames, and then concatenates 4 consecutive predictions to get the result for the 5-frame snippet. In contrast to previous methods, our method also uses stereo in-

Method	Pixel Acc.	Mean Acc.	Mean IoU	f.w. IoU
(Yang et al. 2018)	0.89	0.75	0.52	0.87
Ours (Full)	0.90	0.82	0.56	0.88

Table 5: Motion segmentation evaluation. The metrics are pixel accuracy, mean pixel accuracy, mean IoU, and frequency weighted IoU.

formation. We can see that the rigid alignment module significantly improves the pose estimation (Ego+align vs. Egomotion). After training with the flow consistency and rigid alignment modules, ours (full) model further improves and reaches the performance of state-of-the-art methods.

The other metric is proposed in (Zhan et al. 2018) which measures the average translational and rotational errors for all sub-sequences of length (100, 200, ..., 800). We concatenate all of two frames estimations together for the entire sequence without any post-processing. The results are shown in Table. 4. Our full method outperforms (Zhan et al. 2018) by a large margin, but still falls behind ORB-SLAM (Full) which does bundle adjustments.

Motion Segmentation Evaluation The motion segmentation task is evaluated using the object map provided by the KITTI 2015 dataset. The objects labeled in the object map are treated as moving foregrounds, while all of the remaining pixels are treated as static backgrounds. The metrics follow the ones used in (Yang et al. 2018). We achieve modest improvements in the mean pixel accuracy and mean IoU metrics as shown in Table. 5. The qualitative results of our estimated motion segmentation can be seen in Fig. 5.

Ablation Study The ablation study has already been presented and discussed in previous sections. The comparisons between Ours (Ego-motion), Ours (Ego+align) and Ours (Full) demonstrate the effectiveness of our proposed rigid alignment module and flow consistency module across various tasks of depth, optical flow and odometry estimations.

Discussions

In summary, by mutually leveraging stereo and temporal information, and treating the learning of depth and optical flow as a whole, our proposed method shows substantial improvements on unsupervised learning of depth, optical flow, and motion segmentation on the KITTI dataset. However, there is still a need of future works to continue the improvement.

First, the motion segmentation results are still not good enough for practical usage (see supplementary for more examples). More cues for motion segmentation like the ones used in (Taniai, Sinha, and Sato 2017) might be useful.

Second, due to the limitations of our motion segmentation, we actually did not fully utilize the accurate rigid flow in our optical flow task (see the performance gap between Ours (Ego+align) and Ours (Full) in the rigid regions). If we were able to get a better motion segmentation mask, the KITTI 2015 optical flow task could be further improved.

Finally, although our method handles the moving object explicitly, it still assumes that the majority of the scene is static. More work needs to be done to make it suitable for highly dynamic scenes.

References

- Behl, A.; Jafari, O. H.; Mustikovela, S. K.; Alhaija, H. A.; Rother, C.; and Geiger, A. 2017. Bounding boxes, segmentations and object coordinates: How important is recognition for 3d scene flow estimation in autonomous driving scenarios? In *International Conference on Computer Vision*.
- Besl, P. J., and McKay, N. D. 1992. Method for registration of 3-d shapes. In *Sensor Fusion IV: Control Paradigms and Data Structures*, volume 1611, 586–607. International Society for Optics and Photonics.
- Chang, J.-R., and Chen, Y.-S. 2018. Pyramid stereo matching network. In *Proceedings of the IEEE Conference on Computer Vision and Pattern Recognition*, 5410–5418.
- DeSouza, G. N., and Kak, A. C. 2002. Vision for mobile robot navigation: A survey. *IEEE transactions on pattern analysis and machine intelligence* 24(2):237–267.
- Garg, R.; BG, V. K.; Carneiro, G.; and Reid, I. 2016. Unsupervised cnn for single view depth estimation: Geometry to the rescue. In *European Conference on Computer Vision*, 740–756. Springer.
- Geiger, A.; Lenz, P.; and Urtasun, R. 2012. Are we ready for autonomous driving? the kitti vision benchmark suite. In *Computer Vision and Pattern Recognition (CVPR), 2012 IEEE Conference on*, 3354–3361. IEEE.
- Godard, C.; Mac Aodha, O.; and Brostow, G. J. 2017. Unsupervised monocular depth estimation with left-right consistency. In *CVPR*, volume 2, 7.
- Ilg, E.; Mayer, N.; Saikia, T.; Keuper, M.; Dosovitskiy, A.; and Brox, T. 2017. Flownet 2.0: Evolution of optical flow estimation with deep networks. In *IEEE Conference on Computer Vision and Pattern Recognition (CVPR)*, volume 2.
- Jason, J. Y.; Harley, A. W.; and Derpanis, K. G. 2016. Back to basics: Unsupervised learning of optical flow via brightness constancy and motion smoothness. In *Computer Vision–ECCV 2016 Workshops*, 3–10. Springer.
- Kingma, D., and Ba, J. 2014. Adam: A method for stochastic optimization. *arXiv preprint arXiv:1412.6980*.
- Li, R.; Wang, S.; Long, Z.; and Gu, D. 2017. Undeepvo: Monocular visual odometry through unsupervised deep learning. *arXiv preprint arXiv:1709.06841*.
- Mahjourian, R.; Wicke, M.; and Angelova, A. 2018. Unsupervised learning of depth and ego-motion from monocular video using 3d geometric constraints. In *Proceedings of the IEEE Conference on Computer Vision and Pattern Recognition*.
- Meister, S.; Hur, J.; and Roth, S. 2018. UnFlow: Unsupervised learning of optical flow with a bidirectional census loss. In *AAAI*.
- Menze, M., and Geiger, A. 2015. Object scene flow for autonomous vehicles. In *Proceedings of the IEEE Conference on Computer Vision and Pattern Recognition*, 3061–3070.
- Ranjan, A.; Jampani, V.; Kim, K.; Sun, D.; Wulff, J.; and Black, M. J. 2018. Adversarial collaboration: Joint unsupervised learning of depth, camera motion, optical flow and motion segmentation. *arXiv preprint arXiv:1805.09806*.
- Ren, Z.; Yan, J.; Ni, B.; Liu, B.; Yang, X.; and Zha, H. 2017. Unsupervised deep learning for optical flow estimation. In *AAAI*, 1495–1501.
- Sun, D.; Yang, X.; Liu, M.-Y.; and Kautz, J. 2017. Pwc-net: Cnns for optical flow using pyramid, warping, and cost volume. *arXiv preprint arXiv:1709.02371*.
- Taniai, T.; Sinha, S. N.; and Sato, Y. 2017. Fast multi-frame stereo scene flow with motion segmentation. In *Computer Vision and Pattern Recognition (CVPR), 2017 IEEE Conference on*, 6891–6900. IEEE.
- Tsai, Y.-H.; Yang, M.-H.; and Black, M. J. 2016. Video segmentation via object flow. In *Proceedings of the IEEE Conference on Computer Vision and Pattern Recognition*, 3899–3908.
- Vedula, S.; Baker, S.; Rander, P.; Collins, R.; and Kanade, T. 1999. Three-dimensional scene flow. In *Computer Vision, 1999. The Proceedings of the Seventh IEEE International Conference on*, volume 2, 722–729. IEEE.
- Wang, C., and Buenaposada, J. M. 2018. Learning depth from monocular videos using direct methods. In *Proceedings of the IEEE Conference on Computer Vision and Pattern Recognition*.
- Wang, Y.; Yang, Y.; Yang, Z.; Zhao, L.; and Xu, W. 2018. Occlusion aware unsupervised learning of optical flow. In *Proceedings of the IEEE Conference on Computer Vision and Pattern Recognition*, 4884–4893.
- Wulff, J.; Sevilla-Lara, L.; and Black, M. J. 2017. Optical flow in mostly rigid scenes. In *The IEEE Conference on Computer Vision and Pattern Recognition (CVPR)*.
- Yang, Z.; Wang, P.; Xu, W.; Zhao, L.; and Nevatia, R. 2017. Unsupervised learning of geometry with edge-aware depth-normal consistency. *arXiv preprint arXiv:1711.03665*.
- Yang, Z.; Wang, P.; Wang, Y.; Xu, W.; and Nevatia, R. 2018. Every pixel counts: Unsupervised geometry learning with holistic 3d motion understanding. *arXiv preprint arXiv:1806.10556*.
- Yin, Z., and Shi, J. 2018. Geonet: Unsupervised learning of dense depth, optical flow and camera pose. In *Proceedings of the IEEE Conference on Computer Vision and Pattern Recognition (CVPR)*, volume 2.
- Zhan, H.; Garg, R.; Weerasekera, C. S.; Li, K.; Agarwal, H.; and Reid, I. 2018. Unsupervised learning of monocular depth estimation and visual odometry with deep feature reconstruction. In *Proceedings of the IEEE Conference on Computer Vision and Pattern Recognition*, 340–349.
- Zhou, C.; Zhang, H.; Shen, X.; and Jia, J. 2017a. Unsupervised learning of stereo matching. In *International Conference on Computer Vision*.
- Zhou, T.; Brown, M.; Snavely, N.; and Lowe, D. G. 2017b. Unsupervised learning of depth and ego-motion from video. In *CVPR*, volume 2, 7.